Quarterly Report: September 2010

Methane Recovery from Hydrate-bearing Sediments

Funding Number: DE-FC26-06NT42963

Submitted By:

J. Carlos Santamarina
Georgia Institute of Technology
School of Civil and Environmental Engineering
Atlanta, GA 30332-0355
Phone: (404)-894.7605
Fax: (404)-894.2278
E-mail: jcs@gatech.edu

Costas Tsouris
Oak Ridge National Laboratory
Georgia Institute of Technology
School of Civil and Environmental Engineering
Atlanta, GA 30332-0373
E-mail: costas.tsouris@ce.gatech.edu

Acknowledgment: This material is based upon work supported by the Department of Energy under Award Number DE-FC26-06NT42963

INTRODUCTION - ANTICIPATED MAIN RESULTS

Goals: Identifying, understanding and modeling processes involved in methane production from hydrate-bearing sediments.

Approach: observation and interpretation of phenomena at multiple scales, ranging from pore-contact scale to the macro-reservoir scale, taking into consideration various possible driving forces (e.g., depressurization, thermal stimulation).

Anticipated results and most significant contributions: In view of our experience accumulated since the beginning of the project, we anticipate that some of the main results from this study will address:

- *Hydrate formation and growth*. Different conditions (unsaturated from gas phase, from ice, from dissolved phase, in water-wet and oil-wet sediments, during gas exchange). Formation rates at gas-water interface. Transients. Spatial distribution (partial pore filling, cluster, segregated).
- *Relevance to marine and permafrost environments*.
- *Hydrate-mineral bonding and tensile strength*. Implications on the mechanical behavior of hydrate bearing sediments in view of production strategies.
- *Gas production by heating and depressurization*. Study in 5m long 1D cell. Experimental study and modeling.
- *Gas production by chemo-driven methods*. Fundamental understanding of CO_2-CH_4 exchange.
- *Gas production by transients*.
- *The role of effective stress* in formation and production.
- *Gas invasion versus gas production* – Evolution of degree of saturation and fluid conduction. Fluid-driven fractures.
- *Fluid conductivity in spatially varying sediments*
- *Thermodynamic formulation*
- *Coupled Thermo- Hydro- Chemo-Mechanical formulation*.
- *Production strategies in different formations*
- *Relevance to real systems*

Research Team: The current team is shown next.

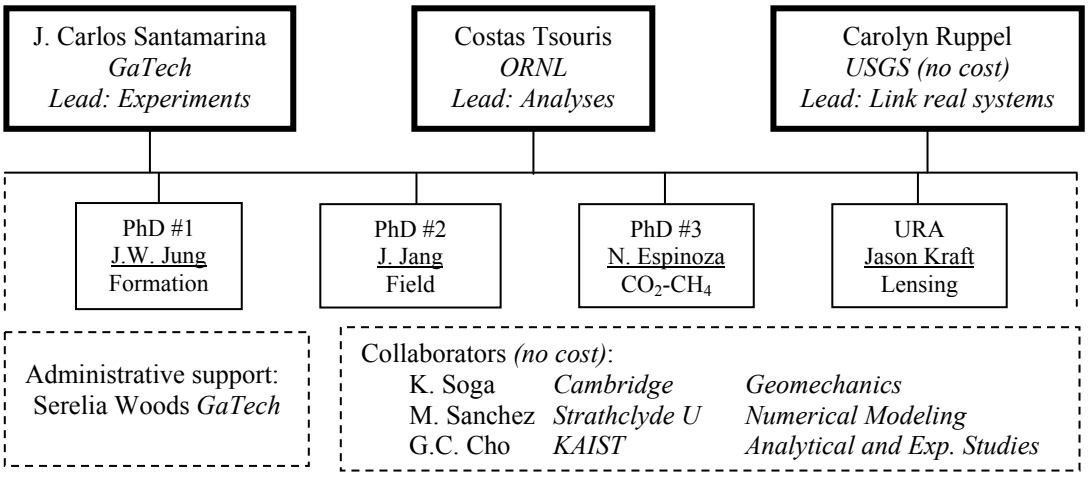

SUMMARY OF RESEARCH DEVELOPMENTS DURING THIS QUARTER

During this quarter, the research team has been dedicated to completing test sequences, advancing analyses, simulating numerical modeling and preparing manuscripts for all tasks reported in previous quarterly reports. The most relevant themes have included:

- Stress-strain response of hydrate-bearing sediments - DEM simulation
  - Particle/packing generation
  - Characteristic behavior, both (1) distributed hydrate and (2) patchy hydrate bearing sediment
  - Comparison of DEM results with experimental data
  - Deformation during hydrate dissociation and gas production

- Relative water and gas permeability in view of CH_4 production
  - Relative water and gas permeability at different hydrate saturation
  - Trapping effects on characteristic curve and relative permeability
  - Evolution of gas and water saturation during gas invasion and nucleation

Both studies are conducted within the context of gas production and recovery efficiency. Details follow

STRESS-STRAIN RESPONSE OF HYDRATE-BEARING SEDIMENTS - DEM SIMULATION

Numerical simulations of a triaxial test are conducted to improve our understanding of the mechanical response of hydrate-bearing sediments, including stiffness, strength, and volumetric dilation, and the evolution during gas production. The following conditions are modeled: (a) sediments without hydrate, (b) distributed hydrate, and (c) patchy hydrate saturation (c1 shows a 2D schematic; c2 shows grain clusters in 3D). In the later, clusters have 100% hydrate saturation while the sediment matrix has no hydrate (transparent in figure c2).

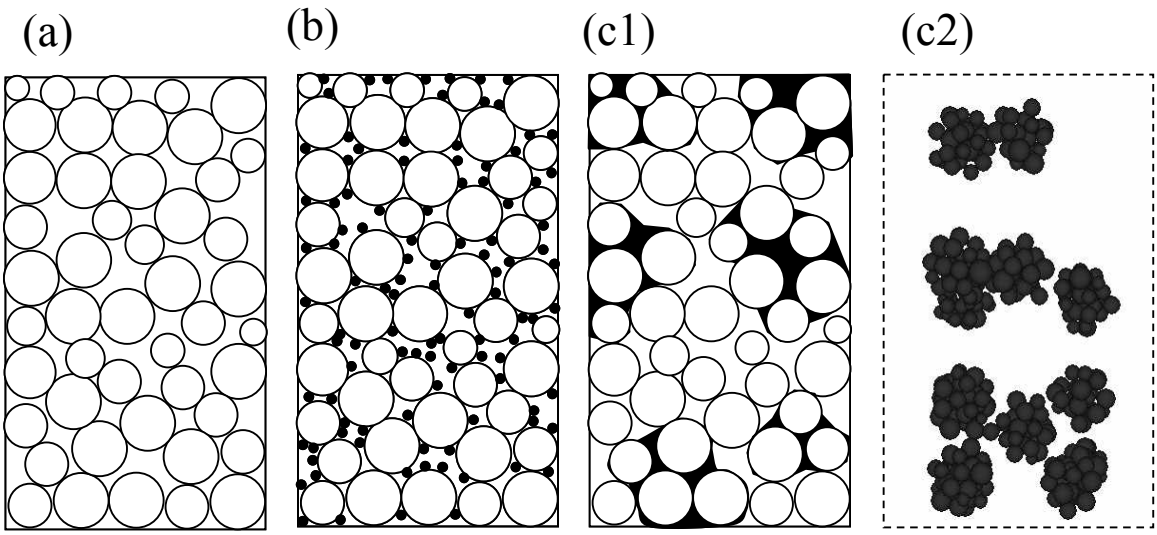

Distributed hydrate bearing sediment (hydrate saturation S_{hyd}). The following figure shows: (a) stress-strain response, (b) volume change, and the p'qe response projected on (c) q-p' plane, and on the (d) e-p' plane. Note: the confining stress is 1 MPa.

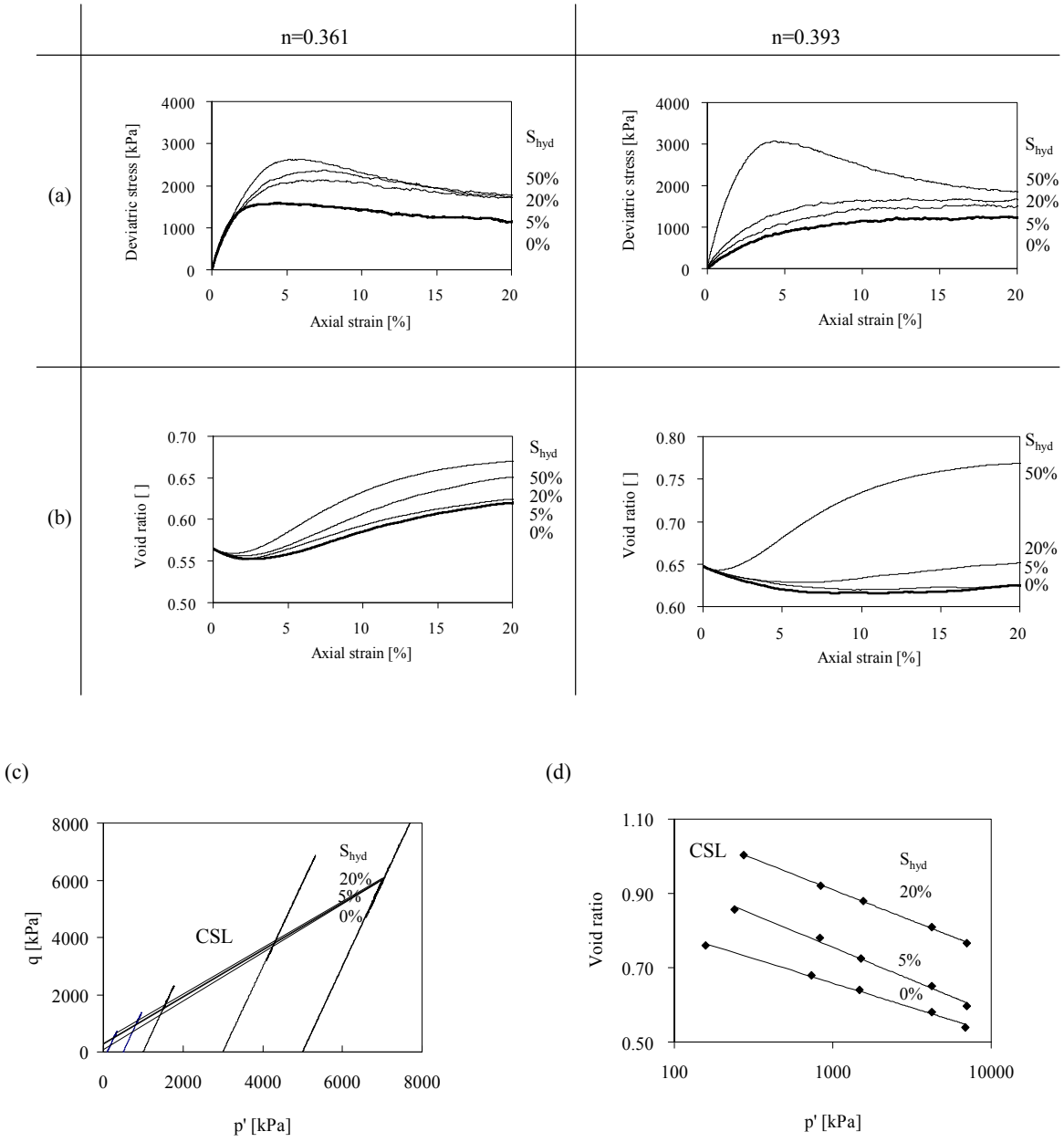

Sediment with patchy hydrate saturation (hydrate saturation S_{hyd}; 15 clusters). The following figure shows: (a) stress-strain response, (b) volume change, and the p'qe response projected on (c) q-p' plane, and on the (d) e-p' plane. Note: the confining stress is 1 MPa.

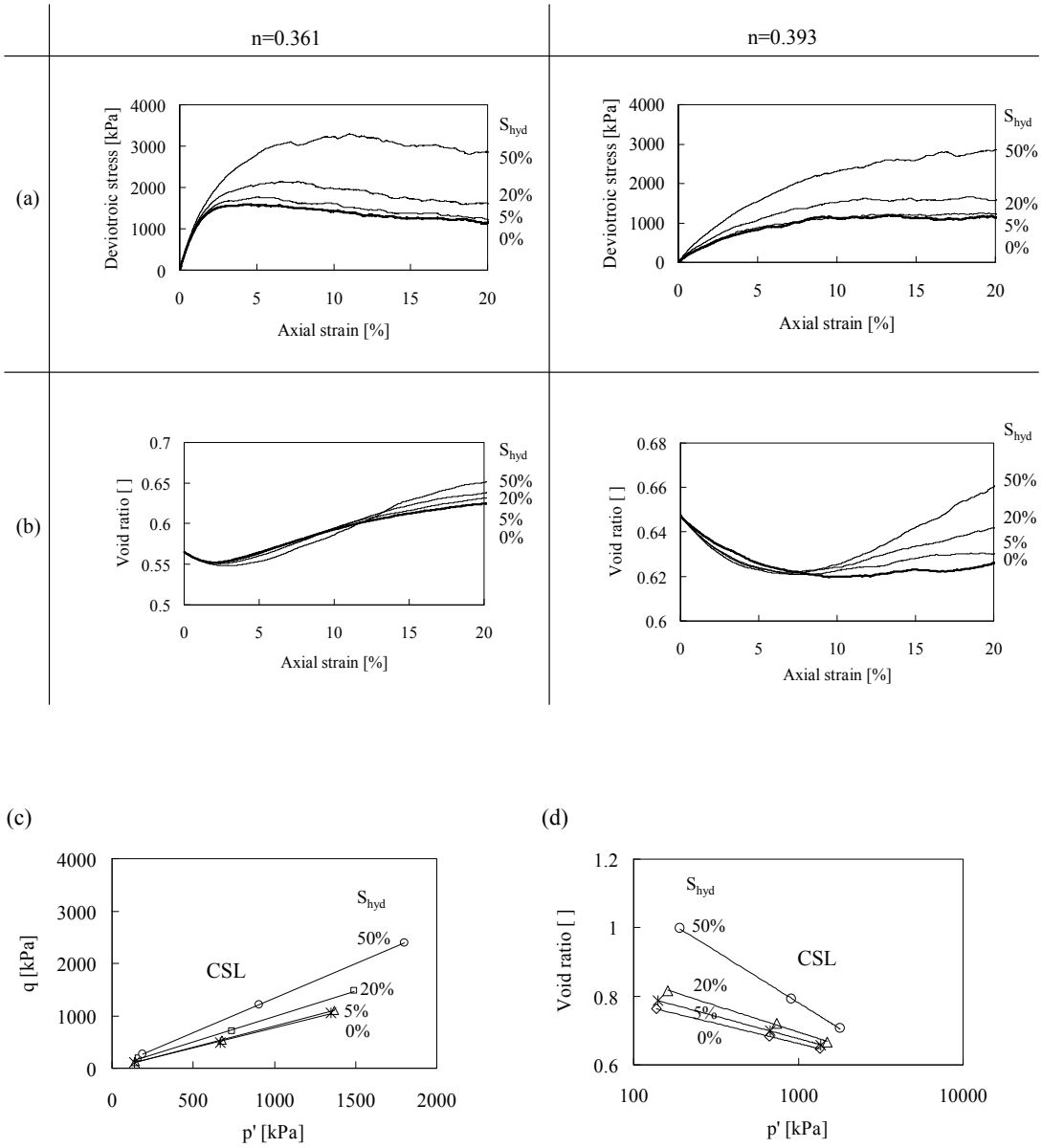

Strength comparison between distributed hydrate-bearing sediments and patchy hydrate. This figure compares results for all simulations conducted at different porosities, hydrate saturations and confinements, for both distributed and patchy saturation.

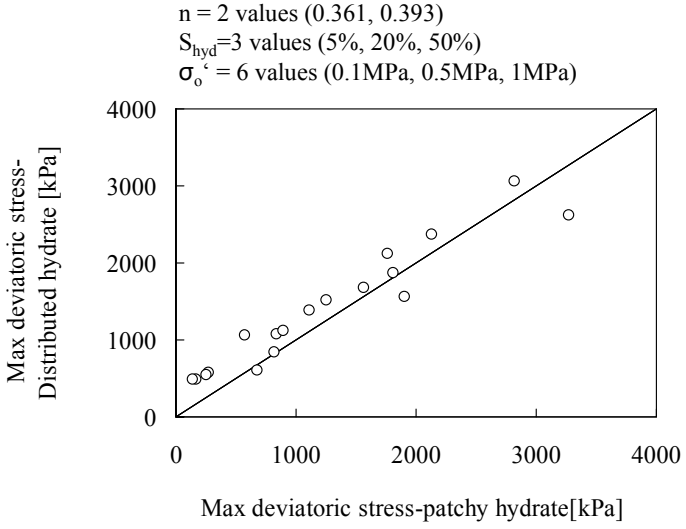

Strength of hydrate-bearing sediments - Experimental data and DEM results. Experimental results published in the literature and numerical predictions using DEM simulations are compared next.

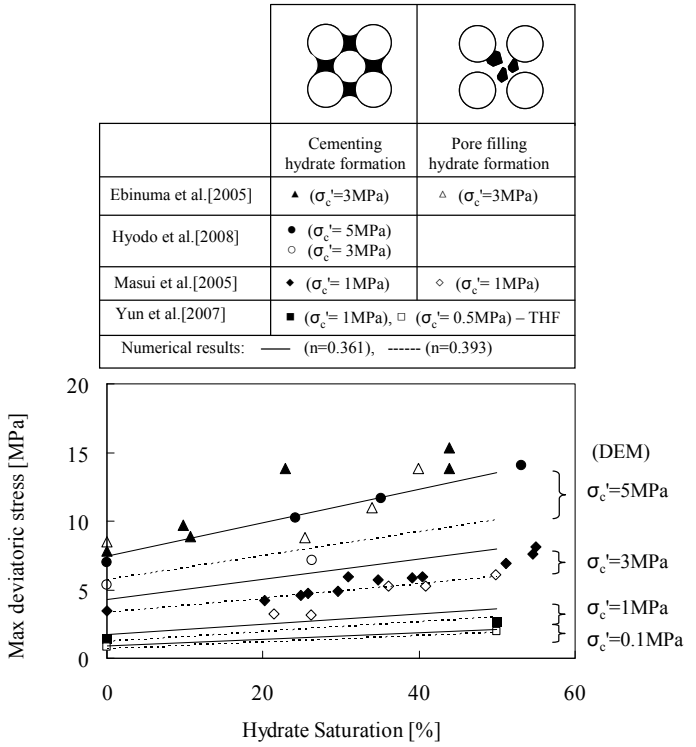

Contact force chains between soil particles. Force chains are compared to understand differences in behavior. Images are shown (a) after consolidation to 1 MPa without hydrate, and after an additional 1.2MPa deviatoric stress is applied to (b) the sediment without hydrate, (c) the distributed hydrate-bearing sediments, and (d) the hydrate-bearing sediments with patchy saturation.

(a) Isotropic load (σ_o=1MPa, σ_d=0MPa)	Under deviatoric load (σ_o=1MPa, σ_d=1.2MPa)		
	(b) Hydrate-free sediments	(c) Distributed hydrate (S_h=20%)	(d) Patchy saturated hydrate (S_h=20%)
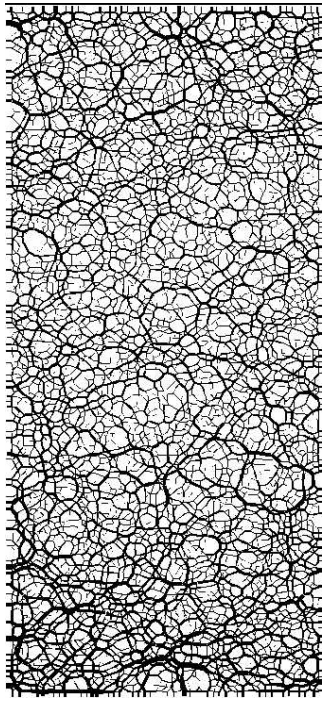	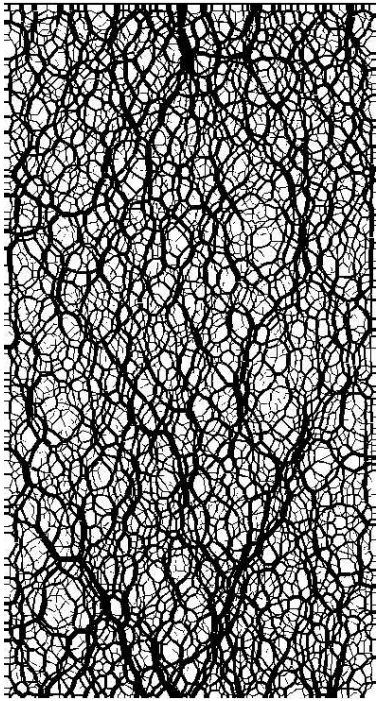	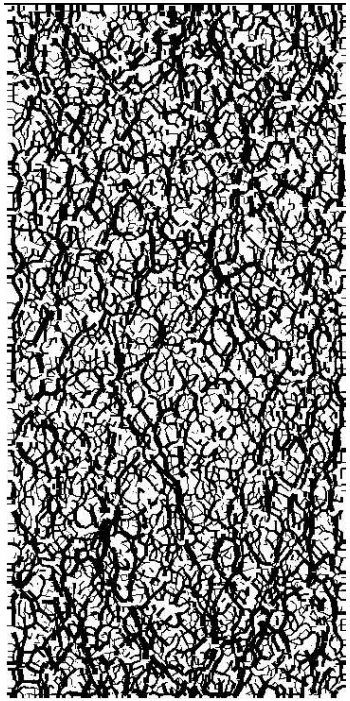	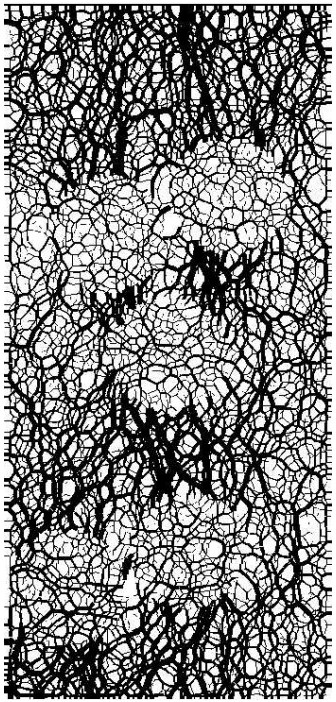

The importance of reservoir boundary conditions on deformation during hydrate dissociation and gas production. (1) constant stress boundary *CS*, (2) zero strain boundary *ZS*, or (3) constant vertical stress but zero lateral strain K_o condition.

(a)

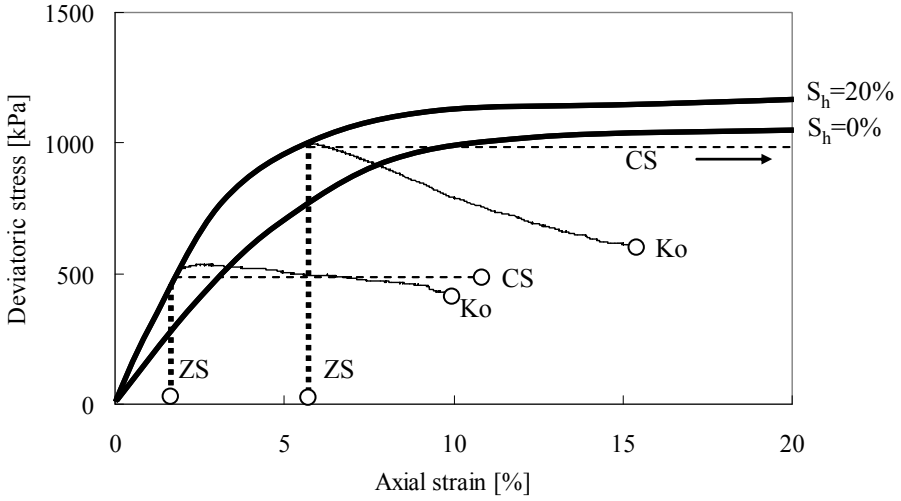

(b)

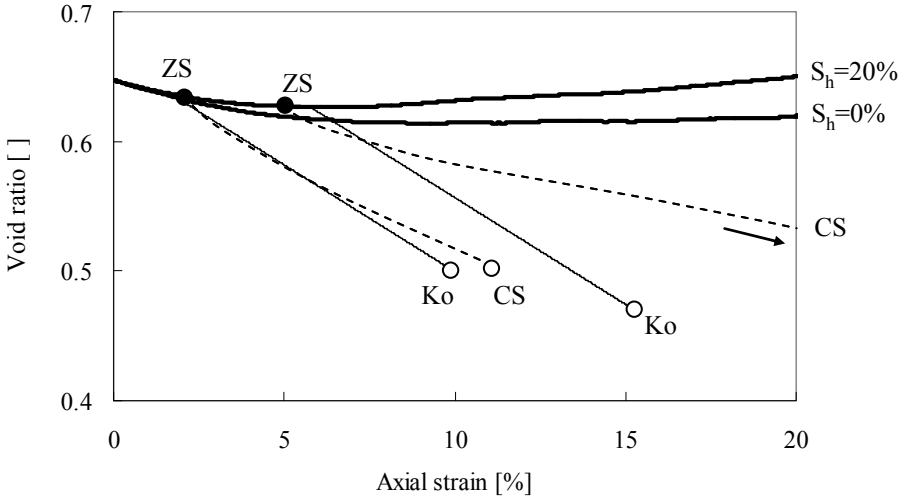

Observations

- DEM numerical simulations provide unique insight into the mechanical response of hydrate-bearing sediments. The hydrate mass can be simulated as either small randomly "distributed hydrate" or as "patchy saturation", whereby clusters with 100% hydrate saturation are distributed within a hydrate-free sediment.

- Simulation results obtained for both hydrate-bearing sediments show an apparently similar global stress-strain response and reveal that increasing either the initial sediment density or the degree of hydrate saturation causes an increase in stiffness, strength and dilative tendency. The combined effects on strength and dilation cause a shift in the critical state line toward higher void ratios and higher p'-q values.

- The strength of sediments with patchy hydrate saturation is slightly lower than the strength of evenly distributed hydrate-bearing sediments.

- Distributed hydrate-bearing sediments exhibit high dilation at low confinement; and a cohesive intercept is obtained when the Coulomb failure envelope is extrapolated to the origin. Yet, hydrate content has almost no effect on critical state friction ϕ_{cs}.

- Sediments with patchy hydrate saturation exhibit delayed dilation until a strain-level that is comparable to dilation in hydrate-free sediments. There is a significant increase in critical state friction angle no cohesive intercept in the p'-q projection.

- Internal particle-scale analyses using normal contact force chains provide unique insight into the different stress responses of both hydrate-bearing sediments. Load transfers are concentrated along stiffer hydrate-filled regions. Hydrate particles bonded onto the mineral surface contribute to increased shear resistance by contiguous particles being bonded together, and by promoting rotational frustration. The strong, hydrate-saturated patches force the development of tortuous rather than planar shear planes and higher energy is required to shear the specimen.

RELATIVE WATER AND GAS PERMEABILITY – ANALYTICAL AND NUMERICAL STUDY

Tube- and pore-network models have been developed and used to explore phenomena related to gas production, including gas nucleation, gas invasion, and gas recovery from hydrate bearing sediments.

The figure shows: (a) the model topologies. (b) Displacement mechanisms. and (c) trapping. The trapping algorithm (tight trapping vs. loose trapping) defines whether a tube filled with the defending phase with invading phase on both ends can be invaded or not. Piston-type displacement is adopted in this study.

(a) Model description

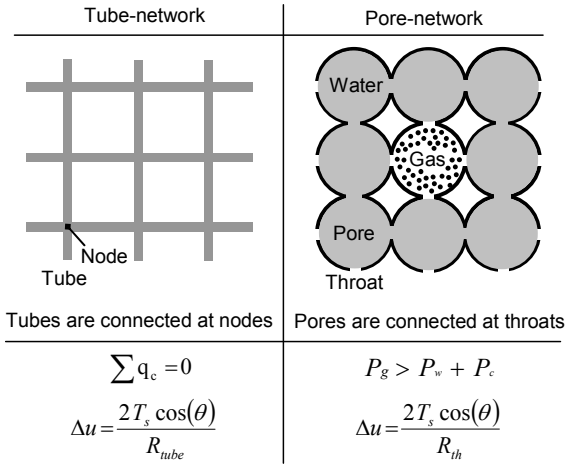

(b) Displacement mechanism

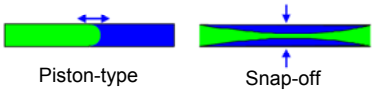

(c) Trapping algorithm

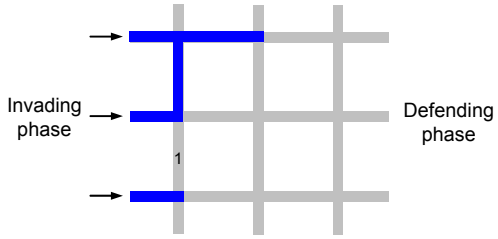

Relative water permeability at different hydrate saturations. Several models for water permeability at different hydrate saturations are compiled and listed in this table. The *N*–parameter in the empirical model depends on the method of hydrate formation in laboratory.

Table. Relative water permeability k_{rw} as a function of hydrate saturation S_h.

	Equations	Factors and explanation	References
Tube-model	$k_{rw} = (1 - S_h)^2 = S_w^2$	Tube coating	Kleinberg et al. (2003) Kumar et al. (2010) Spangenberg (2001)
	$k_{rw} = 1 - S_h^2 + \frac{2(1 - S_h)^2}{\ln(S_h)}$	Tube filling	
Pore-model	$k_{rw} = (1 - S_h)^{n+1} = S_w^{n+1}$	Pore coating n=1.5 ($0<S_h<0.8$) n>1.5 (S_h>0.8)	
	$k_{rw} = \frac{(1 - S_h)^{n+2}}{(1 + S_h^{0.5})^2}$	Pore filling n=0.7S_h+0.3	
Empirical model	$k_{rw} = (1 - S_h)^N = S_w^N$	N=2.6 (obtained from experiment - connate water)	Minagawa et al. (2004)
		N=9.8 (obtained from experiment -gas diffusion)	
		N=2 (used for MH21-HYDRES)	Konno et al. (2010)
		N=10.384S_h^2-27.773S_h+13.639 ($0<S_h<0.3$) (obtained from experiment)	Sakamoto et al. (2007)
		N=3 (S_h<0.35) N=4,5 (S_h=0.42,0.49) (obtained from experiment using gas conductivity)	Kumar et al. (2010)

A three-dimensional tube-network model is used to simulate water conductivity for different degrees of hydrate saturation and hydrate distribution habit. Numerical results and predictions based on the equations tabulated above are compared in the following figure.

(a) Numerical results obtained with capillary tube model (13×13×13 nodes, 3575 tubes, $\sigma(\ln(R/[\mu m])=0.4$). The cases include ① closure from largest tube, ② random closure, and ③ closure from smallest tube).

(b) Kozeny-Carman equation for pore coating and pore filling situation.

(c) Empirical equation.

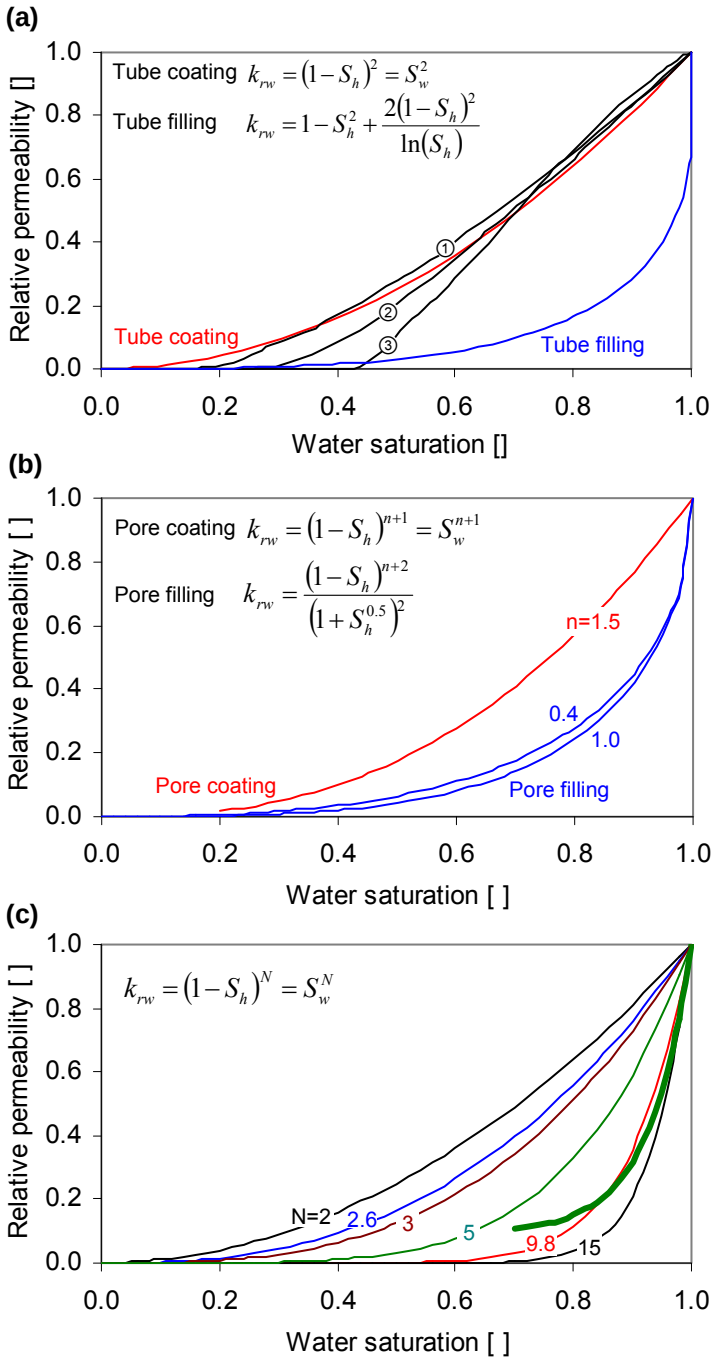

Relative water and gas permeability at different water saturations. Models for relative water/gas permeability at different water/gas saturations are compiled. next

Table. Relative permeability at different saturations.

	Equations	Factors and explanation	References
van Genuchten	$k_{rw}=\overline{S}_w^{0.5}\left[1-\left(1-\overline{S}_w^{1/m}\right)^m\right]^2$ $k_{rg}=\sqrt{1-\overline{S}_w}\left(1-\overline{S}_w^{1/m}\right)^{2m}$ $\overline{S}_w=\frac{S_w-S_r}{1-S_r}$	m=0.46, S_r=0.09 S_r: irreducible water saturation	van Genuchten (1980) Parker et al. (1987)
		m=0.45, S_{wr}=0.2, S_{gr}=0.05	Hong and Pooladi-Davish (2003) Uddin et al. (2008)
		m=0.45, S_r=0.1	Moridis (1998)
Corey	$k_{rw}=\left(\frac{S_w-S_{rw}}{1-S_{rw}}\right)^4$ $k_{rg}=\left(1-\frac{S_w-S_{rw}}{S_m-S_{rw}}\right)^2\left(1-\left(\frac{S_w-S_{rw}}{1-S_{rw}}\right)^2\right)$	S_m=1	Corey (1954)
		$\overline{S}=\frac{S_w-S_{rw}}{1-S_{rw}-S_{rg}}$	Nazridoust and Ahmadi (2007)
modified Stone / Brooks-Corey	$k_{rw}=\left(\frac{S_w-S_{rw}}{1-S_{rw}}\right)^n$ $k_{rg}=\left(\frac{S_g-S_{rg}}{1-S_{rg}}\right)^n$	n=3, S_{rw}=0.15, S_{rg}=0.05 (Hydrate ResSim)	Gamwo and Liu (2010)
		n=4, S_{rw}=0.20, S_{rg}=0.02	Reagan and Moridis (2008) EOSHYDR
		n=3, S_{rw}=0.25, S_{rg}=0.02 (Class 1, Depressurization, k=4.3×10^{-14}m^2, 10^{-12}m^2)	Moridis and Kowalsky (2005) Moridis et al. (2007)
		n=3.572, S_{rw}=0.25, S_{rg}=0.02 (Class 2, Depressurization, k=7.5×10^{-13}m^2)	Moridis and Reagan (2007)a
		n=3.572, S_{rw}=0.25, S_{rg}=0.02 (Class 3, Depressurization, k=7.5×10^{-13}m^2)	Moridis and Reagan (2007)b
		n=4, S_{rw}=0.2, S_{rg}=0.02 (Class 4, Depressurization, k=10^{-15}m^2=*1mD*)	Moridis and Sloan (2007)
		n=4, S_{rw}=0.2, S_{rg}=0.02 n=3.572, S_{rw}=0.25, S_{rg}=0.02	Rutqvist and Moridis (2007)
		n=4, S_{rw}=0.2, S_{rg}=0.02	Reagan and Moridis (2008) Rutqvist and Moridis (2009)
		n=3.572, S_{rw}=0.25, S_{rg}=0.02 (Korea East Sea, k=0.5×10^{-13}m^2=*0.5D*)	Moridis et al. (2009)
	$k_{rw}=\left(\frac{S_w-S_{rw}}{1-S_{rg}-S_{rw}}\right)^{n_w}$ $k_{rg}=\left(\frac{S_g-S_{rg}}{1-S_{rg}-S_{rw}}\right)^{n_g}$	n_g=3 or 4, S_{rw} = 0.12 (fitting from experiment)	Gupta (2007)
Grant	$k_{rw}=\overline{S}^4$ $k_{rg}=1-k_{rw}$	$\overline{S}=\frac{S_w-S_{rw}}{1-S_{rw}-S_{rg}}$	Grant (1977)
Fatt	$k_{rw}=\overline{S}^3$ $k_{rg}=\left(1-\overline{S}\right)^3$	$\overline{S}=\frac{S_w-S_{rw}}{1-S_{rw}}$	Fatt and Klikoff (1959)
Verma	$k_{rw}=\overline{S}^3$ $k_{rg}=A+B\overline{S}+C\overline{S}^3$	$\overline{S}=\frac{S_w-S_{rw}}{S_{mw}-S_{rw}}$ A=1.259, B=-1.7615, C=0.5089, S_{rw}=0.5, S_{mw}=0.895	Verma et al. (1985)

Relative water and gas permeability trends calculated using equations tabulated above are plotted next as a function of water saturation.

(a) van Genuchten model for different coefficients m=0.46, 0.6, 0.8, and 1.

(b) Comparison of Corey's and Stone's models. Parameter is n=3.572 for Stone's model (If n=4, the relative water permeability values obtained by Corey's and Stone's model are identical).

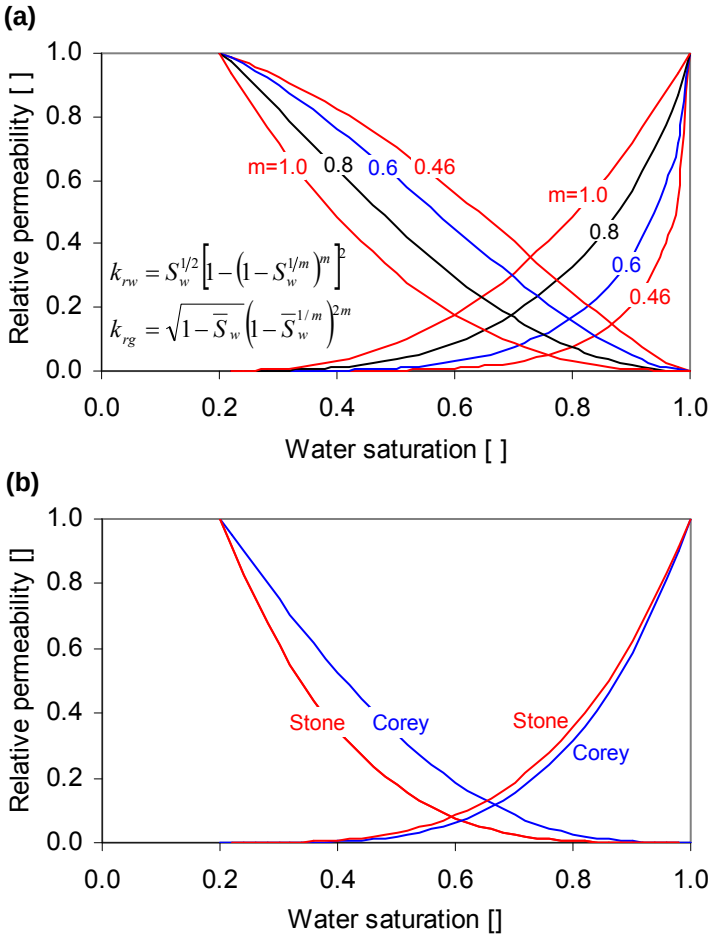

The effect of trapping algorithm on characteristic curve and relative permeability. The effect of tight and loose trapping algorithms on the resulting characteristic curve and relative permeability is studied using network model simulation. The figure shows:

(a) Characteristic curve. Tight trapping has a marked residual saturation.

(b) Relative water and gas permeability. The relative water permeability is similar in both cases, but the relative gas permeability obtained by loose trapping is much higher than that obtained by tight trapping. Also, notice the different residual gas saturation. The gas percolation threshold (where gas is the invading phase) is similar for the two algorithms $S_w \approx 0.85$.

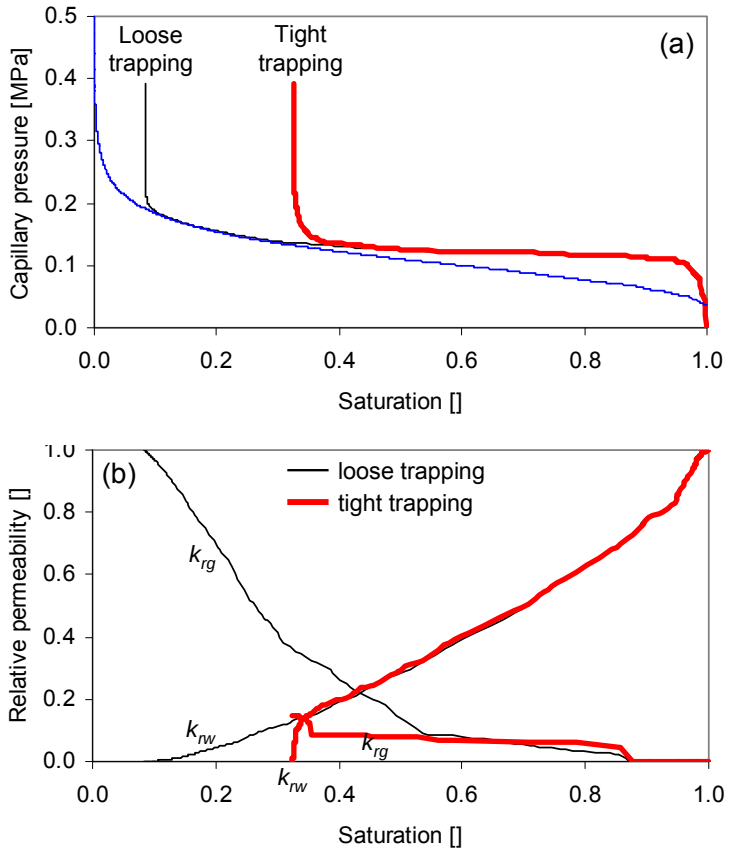

Evolution of gas and water saturation during gas invasion and nucleation. Gas invasion and nucleation processes are simulated using tube-network models. In order to facilitate the visual interpretation, results are shown for two-dimensional network models. The same network is used for gas invasion and gas nucleation. Red circles show the nodes where gas invades or nucleates. The line thickness represents the radius of tubes. (Note: 10×10 nodes, 162 tubes, the number of invasion node is 10).

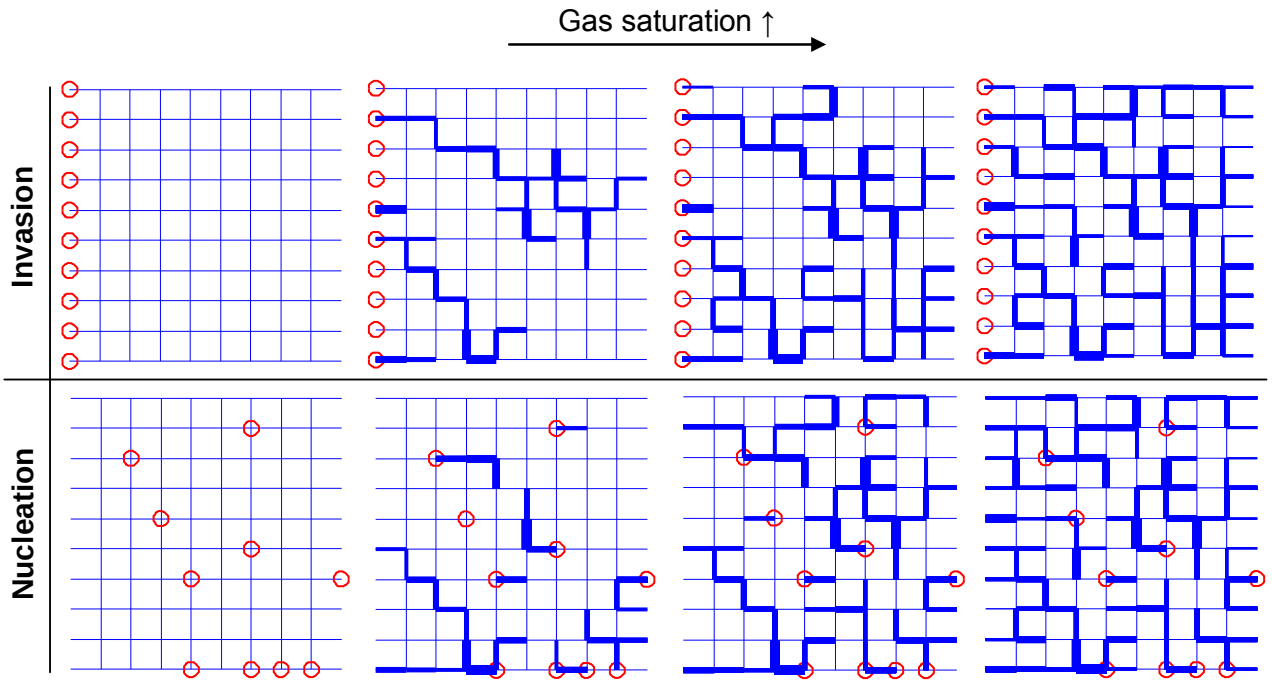

Characteristic curve and relative permeability during gas invasion and nucleation. Gas invasion and gas nucleation lead to different characteristic curves and relative permeabilities. The following results are obtained using a three-dimensional tube-network model with the following characteristics: 13×13×13 nodes, 5460 tubes, coordination number cn=6, log-normal distribution of tube radius R, the mean tube size μ(R)=1μm, and the standard deviation in tube radius σ(ln(R/[μm]))=0.4. Tight trapping algorithm is used. Results follow:

(a) Characteristic curves for spatially uncorrelated random-distributed pores. Symbols: (- black) gas invasion through 13^2 nodes on one side, (- green) gas invasion into the network sorted by tube size; gas invasion through multiple nodes distributed inside network model: (□) 0.5×13^2 and (Δ) 13^2 nodes.

(b) Gas and water conductivity during gas invasion and nucleation are calculated at different saturations. There is noticeable difference in gas permeability obtained by gas invasion and gas nucleation simulation.